A Haptic Continuum Interface for the Teleoperation of Extensible Continuum Manipulators

Chase G. Frazelle[1], *Student Member*, *IEEE*, Apoorva D. Kapadia[1], *Member*, *IEEE*, and Ian D. Walker[1], *Fellow*, *IEEE*

***Abstract*—We describe a novel haptic interface designed specifically for the teleoperation of extensible continuum manipulators. The proposed device is based off of, and extends to the haptic domain, a kinematically similar input device for continuum manipulators called the MiniOct. This paper describes the physical design of the new device, the method of creating impedance-type haptic feedback to users, and some of the requirements for implementing this device in a bilateral teleoperation scheme for continuum robots. We report a series of initial experiments to validate the operation of the system, including simulated and real-time conditions. The experimental results show that a user can identify the direction of planar obstacles from the feedback for both virtual and physical environments. Finally, we discuss the challenges for providing feedback to an operator about the state of a teleoperated continuum manipulator.**

***Index Terms*—Continuum Robots, Haptics and Haptic Interfaces, Telerobotics and Teleoperation**

I. Introduction

CONTINUUM robots [1] present a unique control problem due to their unusual structure. Unlike rigid-link robots that feature a discrete set of joints capable of rotating or extending at fixed locations, continuum robots are capable of bending at any point along their backbone. Developed from the biological inspiration of Animal Kingdom structures (tentacles, tongues, and elephant trunks), continuum robots are able to perform a unique range of environmental interactions in comparison to traditional manipulators [2], [3]. Continuum robots have exhibited numerous system designs and applications in a variety of environments [4], [5], [6], [7], [8], [9].

Extensive research has been conducted into the kinematic modeling of continuum robots [10], [11]. Research has also led to approximations of Jacobian models [12] and more exact models such as [13], [14], [15] which allow for responsive real-time implementation. Further advances have been made in the research of the traditional topics for continuum robots including dynamics [16], [17], [18], [19], [20] and control [21], [22], [23], [24], [25]. The topics of dynamics and control are still active areas of research in continuum robotics. While much attention has been given to these aspects of continuum manipulator operation one limiting factor concerning research of the teleoperation of continuum robots has been the lack of intuitive relationships between a human interface and a continuum system, whereby a user can rely on previous knowledge and environmental observations to perform desired tasks.

In the literature, there have been various investigations into the teleoperation of extensible continuum manipulators [26], [27], [28]. These particular works demonstrated useful capabilities in teleoperating continuum robots but each had shortcomings in various aspects, especially concerning intuitive interfacing. These works relied on complex mappings and control schemes in order to bridge a mismatch in kinematics and degrees-of-freedom which do not necessarily present clearly to users. There have been three recent works particularly focused at developing kinematically similar interfaces for this class of robots. In [29], a 3-section, 9 Degree-of-Freedom (DoF) continuum interface was introduced specifically for the teleoperation of continuum manipulators. The high DoF allowed for 1:1 mappings between the device, termed the MiniOct, and 3-section extensible continuum robots. The MiniOct was also shown to be a versatile tool that could serve as an interface for a variety of continuum robots that varied in both scale and actuation type. The continuum interface presented in [30] is a 4 DoF interface capable of mapping to non-extensible 4 DoF continuum robots. The works shows an intuitive correlation between the shape of the master device and the slave device. In [31], a continuum interface geared towards the teleoperation of growing-vine robots is introduced. In addition to the soft nature of the interface, a unique feature of this device is the use of IMUs to measure the curvature of the device, independent of orientation. The interface itself has 2 DoF, with an additional linear potentiometer that controls the growth rate of vine robots. While unidirectional teleoperation has clearly been explored for continuum manipulators, there appears to be no literature on the design or use of haptic interfaces for teleoperating extensible continuum manipulators.

Haptic feedback is the method of providing sensory feedback through touch [32]. Haptic feedback has been repeatedly used in teleoperated surgery in order to provide surgeons with additional insight about tissues and patient vitals [33], [34]. Other work has studied human perception and lessons that can be learned from psychology in order to maximize the information that can be perceived through auxiliary senses

Manuscript received: September, 10, 2019; Revised December, 16, 2019; Accepted January, 7, 2020. This paper was recommended for publication by Editor Paolo Rocco upon evaluation of the Associate Editor and Reviewers' comments. This work was supported in part by the U.S. National Science Foundation under grants IIS-1527165 and IIS-1718075 and in part by a NASA Space Technology Research Fellowship, contract 80NSSC17K0173.

This paper has supplementary downloadable material available at http://ieeexplore.ieee.org, provided by the authors. This includes video recorded experiments relating to the experimental results presented in this paper.

[1]C. G. Frazelle, A. D. Kapadia, and I. D. Walker are with the Dept. of Electrical & Computer Engineering, Clemson University, Clemson SC (cfrazel, akapadi, iwalker)@g.clemson.edu

Digital Object Identifier (DOI): see top of this page.

[35]. While many haptic interfaces exist and have found practical applications [36], these solutions exhibit a mismatch in DoF and kinematics to multi-section extensible continuum manipulators.

The key contribution of this work is the introduction of the first continuum haptic device designed specifically for the teleoperation of extensible continuum manipulators. The haptic device, nicknamed the HaptOct, is a 3-section continuum interface capable of extending and curving each section, independently, in any direction. The key innovation of this design over the previously reported MiniOct is the complete replacement of the measurement and communication side of the MiniOct along with providing the ability to apply controllable opposing forces to the extension and bending of its continuum interface. Also key to the approach is the method for calculating opposing forces to the user using kinematics unique to continuum manipulators and the simplicity of mapping between master and slave devices.

The paper is organized in the following order: Section II describes the design and construction of the HaptOct, as well as details about the materials and hardware utilized. Section III describes the interfacing scheme when using the HaptOct to teleoperate a remote continuum manipulator and some system requirements. In Section IV, a series of experiments are conducted to validate the hardware and proposed teleoperation scheme. Discussion and conclusions are made in Sections V and VI, respectively.

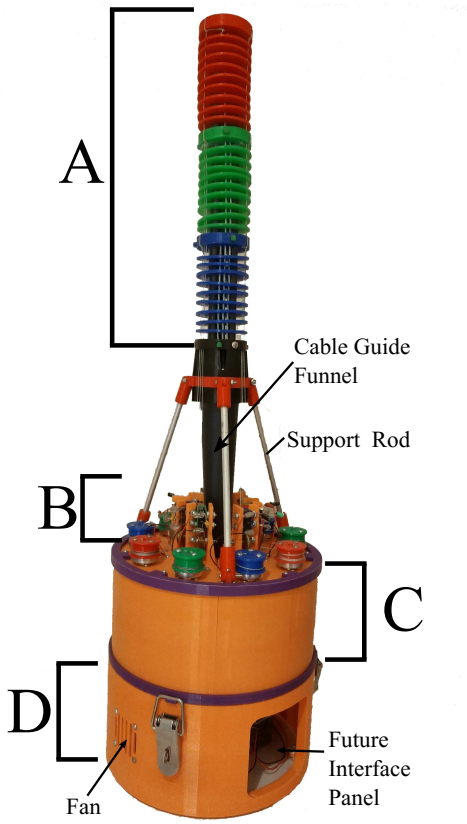

Fig. 1: Haptic Device for Continuum Manipulators

II. System Design

This section details the mechanical and operational design of the proposed continuum haptic input device for teleoperating continuum manipulators. The physical prototype can be seen in Figure 1, where the following text subsections correspond to the labeled areas of the figure.

A. Continuum Interface

The continuum section of this device–the part handled by the user–was first designed for use in the MiniOct, a passive master device explicitly for the unilateral teleoperation of extensible continuum manipulators. The MiniOct's design was chosen as the basis for this new device because of the kinematic and visual similarity between the master device and potential slave systems. The original design details of the continuum interface are described in [29]. As an overview, there are three individual sections, each comprised of a parallel set of extension springs and steel cables that allow an operator to extend and curve each section into a desired configuration. Plastic spacers (9 per section) are distributed evenly along the length of a section and keep the springs and cables uniformly, radially, spaced. The spacers cause any imposed curvature to divide evenly along the length of the section. A spring loaded tab connected to each structural steel cable through the section divider at the base of each section holds the section shape until the operator changes the shape by pressing one of the tabs, releasing the cable, and then extending or shortening the length of the cable. When a tab is subsequently released by the operator, the shape is locked. An illustration of the

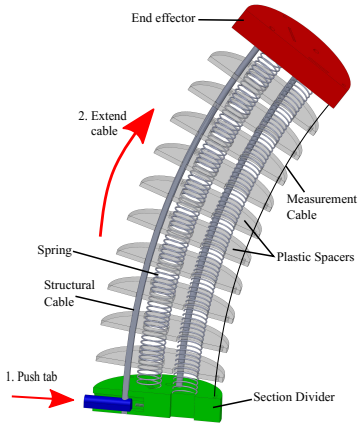

Fig. 2: Basic Operation of Continuum Section

operation of this mechanism is given in Figure 2 while an example of multi-section teleoperation can be seen in Figure 3. The continuum interface is supported via 3 aluminum rods. These rods can be extended or shortened to allow for the storage of longer structural cables. To protect the electronics and device internals in the lower sections of the HaptOct, the stored structural cable is guided by a funnel running through the center of the device (labeled in Figure 1).

B. Configuration Sensing

As with the original MiniOct [29], we use the measured length of three cables (per section) to determine the length

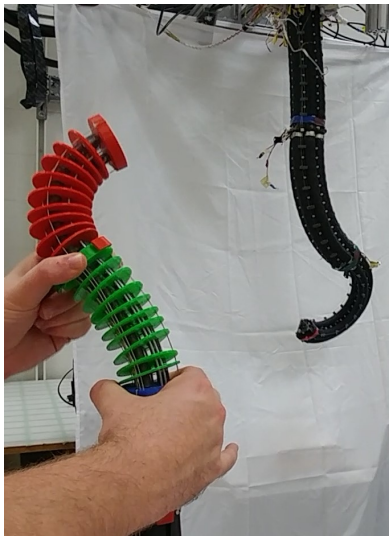

Fig. 3: Teleoperation Between HaptOct (left) and OctArm Manipulator (right)

and shape of each section. As an upgrade to the passive and noisy string potentiometers in the original device, we have replaced each string pot with a combination of an HEDS-5540 series optical encoder and a 25.4mm diameter spool that stores excess cable. The encoders are capable of providing 2000 counts per rotation of the spool, giving a granularity of 39.9μm for each cable. In addition to the spools, a pulley located near each spool helps route the cables from the horizontal orientation of the spool to the extending vertical motion of each section. One advantage of this overall arrangement is the elimination of a maximum extension restriction for the overall device (previously 30cm).

The use of the optical encoder and spool also removes the passive, but increasingly opposing, force of the original spring loaded potentiometers that beneficially removed slack on the measurement cables but also made it harder to extend the MiniOct to full length (a noted issue in [29]). In order to replace the slack collection, we used a solution inspired by slack line detection in industry [37]. As seen in Figure 4, the solution involves placing a micro-limit switch with a roller in line with each measurement tendon just above the routing pulleys. The cover on the switch keeps the tendon pressed against the roller when there is excessive slack and prevents the tendon from falling away from the pulley or out of alignment. When the switch opens, the resulting signal causes the device to take in slack, using the motors described in Section II-C, until the switch closes. Important to the development was the release force of the switches (8.15 grams-force), as a higher release force could potentially turn the spool and open the switch when no actual slack existed on the line. This solution to use limit switches to detect and avoid slack is similarly implemented in [38]. Other recent solutions in continuum robotics to avoid slack such as [39] and [40] require considerably more complex hardware and foot print than the implemented solution herein.

The changes in length recorded by the encoders are then converted via kinematics [41] to shape values that can be used as input for a slave device as with the MiniOct.

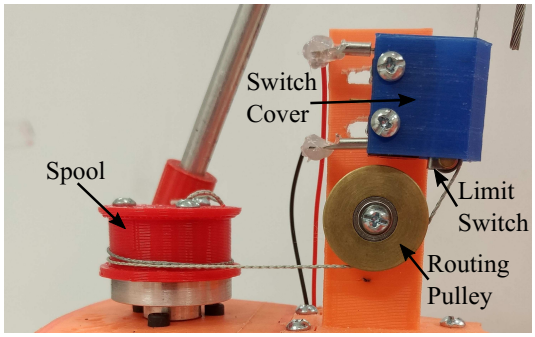

Fig. 4: Limit Switch and Cover for Slack Detection

C. Actuation

The HaptOct acts as an impedance-type haptic device by reflecting opposing forces to an operator in response to extensions of the continuum interface. The medium for these opposing forces is the individual measurement cables in the interface, but the forces themselves are generated by DC motors connected to the measurement cable spools. Each spool is connected to the output shaft of a Maxon Brushless DC Motor (series 273753) by a 6mm Pololu mounting hub. Connected to the opposite end of the motor shafts are the encoders for the measurement cables. All nine motors lack a gearbox connected to the output of the motor, thereby allowing the cable spools to easily turn by hand when unpowered, which is critical for allowing the operator to easily manipulate the continuum interface without unintended resistance. These motors are readily available and have a desirable current-to-torque relationship for our needs. The DC motors are driven by a series of Pololu G2 high power motor drivers, which require a Pulse Width Modulated (PWM) signal and a binary direction signal. Each Maxon motor is mounted to a custom motor mount that encases the entire motor and provides an outlet for the shaft, power cables, and the encoder port.

D. Processing

The core processing of the HaptOct is executed by an Arduino Due which has an Atmel SAM3X8E ARM Cortex-M3 CPU [42]. The board features an 84MHz clock, 12 PWM pins, 42 GPIO pins, and 12 analog input pins. The Due is capable of communication via serial USB, Inter-integrated Circuit (I^2C) protocol, and Serial Peripheral Interface (SPI). We primarily utilize the serial communication and Bluetooth communication through an external Bluetooth module. The Due was ultimately chosen for use because it enabled the HaptOct to achieve an on-board refresh rate of approximately 2.5kHz when interacting with simple virtual obstacles such as virtual surfaces. The refresh rate for bilateral teleoperation between the HaptOct and a slave device is largely limited by the communication protocol, primarily serial USB communication in this case, and the size of communication packets. The refresh rate for the experiments here averaged around 26Hz.

The device is powered by a 40W AC-to-DC converter that supplies an output voltage of 5V. The 5V output directly

powers the Due and 2 DC computer fans that help ventilate the lower sections of the HaptOct. In order to power the motors and motor drivers, the 5V is stepped up to 7.5V using a DC-to-DC converter.

III. System Implementation

The logic and theory that drive the HaptOct are detailed in this section. The device is designed to be an impedance display, which measures movement provided by the operator and exerts a force that can be sensed by the operator [32]. Figure 5 contains the logic flow for the bilateral teleoperation of a three-section continuum manipulator. The vector value l_m represents the lengths of measurement cables of the master device and l_s defines the actuator lengths of the slave device as measured locally by the slave system. These measurements are used to approximate the kinematic values ($q_{m,s}$) for both the master and slave device, respectively, by each system's local controller. The slave controller sends the vector input τ_s to the slave device as calculated by the controller in order to achieve the designated configuration. The vector value F_m is the opposing force experienced by the operator corresponding to an error vector, e_s, produced by the slave system. The error between the master device and tracking slave device is only one component of the total opposing force felt by an operator. The central block, T_{delay}, represents the lag in time experienced between the master and slave device due to transmission over various networks and physical distance between the two devices. In this work, we do not explore the impact of time lag on user experience and assume a negligible round trip delay in our network.

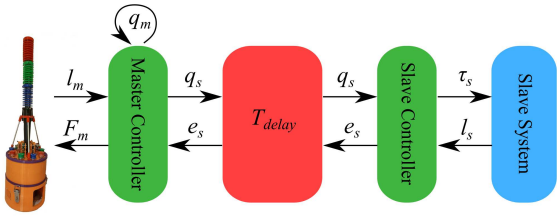

Fig. 5: Teleoperation Scheme for HaptOct

A. Master System

As described in Section II-B, the HaptOct is capable of sensing the lengths of the measuring cables through optical encoders. These lengths are converted to the forward kinematic values (as in [43] and [44]) used for the slave system and scaled to the kinematic range of the slave. Due to the master device having the same kinematic structure as the slave, we are able to map one-to-one the kinematics of the HaptOct to a slave device during this process. The scaled values are then relayed to the slave system controller.

As previously mentioned, the master system receives the current error seen by the slave system controller. The error values are then used to calculate an error force component which, in addition to other force components, determines the final force experienced by the operator. The reported error can be with respect to either the kinematic values or the actuator level errors (i.e. lengths of tendons/actuators), but the computed output force to the operator is calculated with respect to each individual measurement cable. An example of the relationship between the error, additional force values, and final output force is given by the equation:

$$F_l = C_e\mathbf{e} + C_{\Delta e}\mathbf{\Delta e} + C^{\,max}_{length} f^{\,max}_{length}(l) + ... \quad (1)$$

$$f^{\,max}_{length} = (l - l_{max}) \cdot H(l - l_{max}) \quad (2)$$

where the scalars C_e and $C_{\Delta e}$ are the force coefficients for the slave state error ($\mathbf{e} \in \Re^{9x1}$) and change in error ($\mathbf{\Delta e} \in \Re^{9x1}$), respectively. The equation for the overall opposing force, F_l, for a cable l can be expanded to incorporate additional force terms. For example, $f^{\,max}_{length}$ defined in Eq. 2, and its corresponding coefficient $C^{\,max}_{length}$, exists to prevent the extension of a tendon beyond a predetermined maximum length and thus adds to the overall opposing force F_l only when a cable on the HaptOct is extended beyond a set maximum (as conveyed by the Heaviside step function $H(\cdot)$). This maximum length enforcing term is also smoothed by scaling the force by the extension beyond the maximum length. Additional terms could include forces exerted by a known environment (i.e. an a priori simulated obstacle), or internal forces/dynamics known about the slave device.

In order to provide an example for how the error in configuration between the master and slave device contributes to individual tendon forces, we exploit the kinematic model, detailed in [44]. This model describes a single extensible continuum section by the three values $s(t)$, $u(t)$, and $v(t)$. The value $s(t)$ is the arc-length of the section and $u(t)$ and $v(t)$ represent a rotation about the local z-axis. We have reported previously in [41] the 3-actuator based equations that relate $s(t)$, $u(t)$, and $v(t)$ to tendon or actuator lengths, reproduced here:

$$s(t) = \frac{l_1 + l_2 + l_3}{3} \quad (3)$$

$$u(t) = \frac{l_2 - l_3}{d\sqrt{3}} \quad (4)$$

$$v(t) = \frac{s(t) - l_1}{d} \quad (5)$$

Here, the scalar d is the radial distance between the centerline of the section and each measured length-line. It can be shown that the inverse of these equations (i.e. mapping from $s(t)$, $u(t)$, and $v(t)$ to actuator lengths l_1, l_2, and l_3) are:

$$l_1 = s(t) - d \cdot v(t) \quad (6)$$

$$l_2 = s(t) + \frac{d \cdot v(t)}{2} + \frac{\sqrt{3}d \cdot u(t)}{2} \quad (7)$$

$$l_3 = s(t) + \frac{d \cdot v(t)}{2} - \frac{\sqrt{3}d \cdot u(t)}{2} \quad (8)$$

In observing these equations, we find a unique relationship between each of the three length values and the values $s(t)$, $u(t)$, and $v(t)$, as expected. This can serve as the basis for forces due to arc-length and bending in our system. By extension of these equations, we can calculate unique error values for each individual tendon by comparing the master

configuration with that of the slave. An example of the error term for tendon l_2 is:

$$e_{l_2} = (s_m(t) - s_s(t)) + \frac{v_m(t) - v_s(t)}{2} + \frac{\sqrt{3}(u_m(t) - u_s(t))}{2} \quad (9)$$

where (s_m,u_m,v_m) is the master configuration and (s_s,u_s,v_s) is the slave configuration for a single section. The change in error term ($\mathbf{\Delta e}$) can be computed as the time derivative of this error, relating whether or not the slave is converging to the configuration of the master device. The output force computed from combining the various terms is then converted to a torque exerted by each DC motor as a function of current supplied by an individual motor driver.

B. Slave System

The flow of logic shown in Figure 5 assumes the slave system in this scheme has the ability to converge to a desired configuration through closed-loop control and can monitor and communicate error as the system converges or diverges. As in [29], potential slave systems for this scheme can have a variety of actuation methods (pneumatic, tendon, etc.) and different proportions or range-of-motion. This flexibility in types of hardware capable of being teleoperated represents an advantage of the proposed device.

IV. Experimental Validation

We completed a series of experiments to validate both the hardware and the teleoperation scheme. The following subsections describe the experiments and results.

The OctArm manipulator [45] serves as the example slave device in a bilateral teleoperation scheme. The OctArm is a pneumatically actuated extensible continuum robot consisting of 3 distinct sections. Each section has the ability to extend along its backbone and bend along orthogonal axes, totaling in 9 DoF for the overall device. The OctArm can be seen in Figure 3 where it is being teleoperated using the HaptOct. In the described experiments, the OctArm is laying on top of a horizontal surface.

A. Maximum Length Enforcement

The first experiment tests the ability of the system to limit the operator from over extending a section (i.e. the impact of f_{length}^{max} in Eq. 1). As a default, the function prevents the master device from extending beyond 100% of the initial length, a feat that most continuum manipulators are incapable of. When designated to drive a particular slave device, the max extension can be scaled to match the range of motion of the slave. For example, OctArm sections can nominally extend an additional 30% beyond their initial lengths.

In this experiment, we constrained the distal section of the master device to match the proportional maximum extension of the OctArm. Given the initial section length of 10cm for the HaptOct (as described in [29]), we set a virtual maximum length of 13cm for each individual measurement cable. We

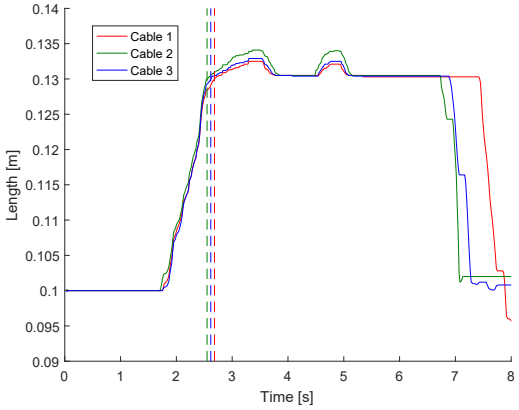

(a) Measurement cable lengths during distal section extension.

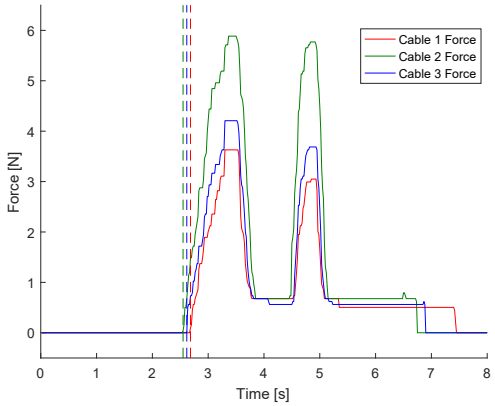

(b) Generated forces corresponding to overextension of distal section.

Fig. 6: Experiment 1, Force output due to extension.

then attempted to extend the section to this threshold and beyond while recording the resulting force exerted by the interface. Figure 6(a) shows the lengths of the three measurement cables and is marked with a vertical dashed line when the lengths first pass the maximum length threshold. Figure 6(b) shows the force exerted, calculated in Newtons, for each of the cables. It can be seen that all three cables react proportionately to their individual displacements beyond the maximum and produce sufficient force to be noticed by the operator (>3N per cable). The difference in time for each cable exceeding that maximum and the difference final maximum between cable tensions can be contributed to the motion by the operator not being pure extension (i.e. the user is lengthening at a slight bending angle). This results in cable 2 in this particular experiment being extended slightly more (between 1 and 2mm) than cables 1 and 3, also resulting in a greater force from the HaptOct.

B. Known Obstacle in Slave Task Space

In the second experiment, we evaluated the ability of the HaptOct to oppose invalid configurations given a priori knowledge of the slave system's environment. In particular, we simulate a scenario in which the slave system is known

to be laying on a planar surface, restricting the valid motions of the robot to configurations curving or extending away from the plane or moving parallel to the surface.

For this experiment, we introduced a new term to the force equation that describes our virtual obstacle. As with Eq. 2, we use the Heaviside step function ($H(\cdot)$) to define simple boundaries and use more complex functions for harder to define boundaries. An example equation for describing a virtual obstacle seen by l_2 is:

$$f_{2_{virt}} = C_u \cdot u(t) \cdot H(u(t) - u_b) + C_v \cdot v(t) \cdot H(v(t) - v_b) \tag{10}$$

where C_u and C_v are the coefficients for the bending displacements $u(t)$ and $v(t)$, respectively, and scalars u_b and v_b serve as simple bounds for $u(t)$ and $v(t)$. The final term $f_{2_{virt}}$ can be added to the total force value defined in Eq 1 for tendon 2. Similar terms are also added to the force equations for tendons 1 and 3.

Now that we have a force expression for bending, we can simulate a planar obstacle for the slave device. We set the bound to be the yz-plane, which correlates to setting a bound on $u(t)$ such that $u(t) \geq 0$. Figure 7(a) shows the values of $u(t)$ and $v(t)$ as the operator attempts to bend and rotate the distal section of the HaptOct in all directions. Figure 7(b) shows the three force values corresponding to the changes in $u(t)$ and $v(t)$. As predicted in Eq. 10, we see a noticeable increase in force response as the operator tries to bend in the positive $u(t)$ direction. Cable 1 does not apply an opposing force to the operator because it is independent of $u(t)$ and there is no restriction on $v(t)$. Cable 3 does have dependency on $u(t)$, but is not permitted to apply negative forces. This shows the HaptOct is capable of opposing operator motion for basic virtual obstacles.

C. Real-time Unknown Obstacle in Slave Task Space

We repeated the previous experiment concerning a slave system placed against a planar surface but removed the a priori knowledge of the surface from our scheme. In this case, we perform real-time bilateral teleoperation and rely on the error between the slave device and master device to convey the planar obstacle to the operator.

As seen in Figure 8(a), the operator in this experiment rotates the HaptOct section in all directions over 4 distinct periods. We can see the relationship between $u(t)$ and $v(t)$ given this plot. In Figure 8(b), we see the corresponding forces experienced by the operator during this repeated motion. At an initial glance, it is difficult to determine the obstacle by the reaction forces alone. However, in Figure 8(c), we see the original motion plot overlaid by the scaled generated forces. As marked by the vertical bars in the plot, it is easy to now see that the periods of time when we have the largest force exerted by each tendon align with the periods when the magnitude of $v(t)$ is positive or nearly positive. The value of $u(t)$ during these same periods spans the entire range of $u(t)$ used by the operator. The operator can conclude from this result that the slave robot is laying in the xz-plane and oriented such that values of $v(t) \geq 0$ result in collision with the plane.

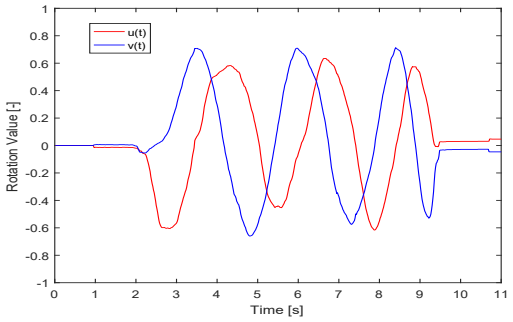

(a) Kinematic values u(t) and v(t) during rotation of distal section.

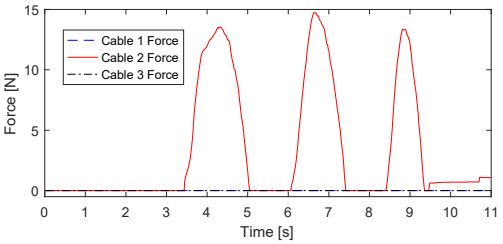

(b) Generated forces corresponding to bending of distal section with known planar obstacle.

Fig. 7: Experiment 2, Force output due to bending.

V. Discussion

The underlying goal of this work was to design and construct a continuum device capable of providing intuitive haptic feedback to an operator while teleoperating a wide range of continuum manipulators. Much of the design work has been completed and presented here but further testing remains necessary to validate the long term success of this strategy.

There were numerous constraints that influenced the design of the mechanism. First, the system needed to minimize resistance to motion seen by the operator when there is no acting force from the device. This led to the use of DC motors without a gear system. This reduces the maximum opposing force the system can exert but gives the least inherent resistance. Second was the desire to develop a compact device that did not have an overly bulky actuator package. As depicted in Figure 1, the complete actuator package, logic, and power supply measures 20.3cm in diameter and 30.9cm in height. Another constraint was the desire for intuitive feedback, both visual and haptic, which led to the use of the kinematically similar three section MiniOct design as the base for developing a haptic device.

In the initial stages of developing this device, choosing the mode of feedback for developing a new haptic device was a cost and reward driven process. As mentioned in [32], tactile and vibrotactile feedback are common modes. We determined that for an initial investigation, the process of creating a synthetic skin for the continuum device, while intriguing, would likely be very difficult to realistically achieve and keep the device portable and relatively simple. The tactile interface would likely be very useful for conveying contact between the slave system and the environment, but would also require a significant amount of information about the slave system

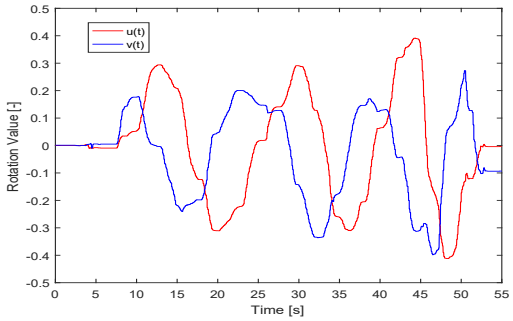

(a) Kinematic values u(t) and v(t) during rotation of distal section.

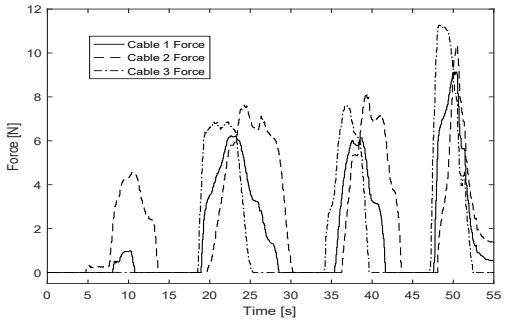

(b) Generated forces corresponding to bending of distal section with unknown planar obstacle.

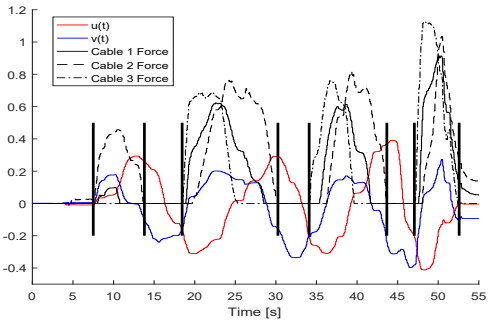

(c) Combined scaled plot of positions and forces.

Fig. 8: Experiment 3 Results, Observing unknown obstacles.

in order to accurately portray points of contact. Vibrotactile feedback was much easier to envision as the actuators are relatively small and would likely only require simple error models. A drawback of a vibrotactile mode would be the need to run wires through continuum sections and it could prove difficult to localize the vibration to a single side of the device or single section for a multi-section system. An admittance feedback device was not investigated in detail, but could prove to be an area of future exploration.

Through initial testing of the device and observations about the design of the system, there are some improvements that can be made to the current design. As with many bilateral teleoperation schemes, the performance of the operator and their ability to perceive mismatches between the master and slave device can depend on the refresh rate and lag experienced by the operator. Initial tests on a local system using serial communication has achieved a round trip refresh rate of 26Hz, the delay from which will likely be noticed by the user. A proposed solution to this will be to use a faster mode of communication, such as SPI or I2C for local communication. As mentioned in Section II-D, the HaptOct as a standalone device has an average refresh rate above 2.5kHz, which provides opportunity for the development of more complex virtual environments that do not rely on communication lags while maintaining smooth operation. When performing the experiments over a distance of hundreds of miles (performed from Houston, Texas to Clemson, South Carolina in the U.S.A.) we experienced a lag of approximately 0.1 seconds. We did not analyze the impact of this delay on performance, though it was negligible enough to perform the experiments and collect the results presented in Sections IV-B and IV-C. Future work can now explore appropriate means for addressing lag of varying severity.

Another limitation is that the device can only oppose the operator when extending any one of the three sides of the device. The limitation arises from the fact that the device always inherently assumes that the slave system can retract or straighten from an extended or curved configuration. This assumption is not that disruptive in a static environment, but could prove erroneous for dynamic environments in which a slave system might become trapped.

The largest challenge for this haptic device (and any haptic device with regards to continuum manipulators) is the conclusion that the feedback is only as informative and accurate as the error model that is available for the slave system. One example of this could be a scenario in which a distal section of a slave system has come in contact with an object, but is able to bend or extend normally. However, the proximal sections begin to curve due to the compliant nature of continuum robots. The operator may not perceive this deformation until attempting to later manipulate the proximal section. Another scenario particular to pneumatically actuated continuum manipulators is the increase in stiffness of a muscle as it is extended. This internal stiffness may be difficult to detect through error modeling, but would be useful feedback for the operator to know that the system is approaching its physical limits.

In addition to addressing many of the issues noted here, it is the goal of future work to further evaluate the current design and compare this device to other haptic interfaces. It will also be an interesting challenge to see how forces can best be routed through proximal sections.

VI. Conclusion

The first continuum haptic device specifically designed for the teleoperation of continuum manipulators was explored and prototyped. An overview of the physical design and features of the device is given, including the assumptions and needs for the successful implementation of bilateral teleoperation for continuum manipulators. Through a series of experiments, we showed that the device and the force based model performed as intended by exerting opposing forces to the operator in the response to known and unknown constraints for the slave device. We discussed the specific challenges of continuum manipulators for haptics, such as the need for suitable error

models in order to display to an operator the different interactions a slave system has with its local environment and internal constraints. Future work will look to improve error modeling, the development of virtual test environments, and addressing teleoperation challenges such as communication lag and refresh rate.

REFERENCES

[1] G. Robinson and J. Davies, "Continuum robots - a state of the art," in *Proc. IEEE Int. Conf. Robot. Autom.*, Detroit, MI, 1999, pp. 2849–2854.

[2] R. Webster III and B. A. Jones, "Design and modeling of constant curvature continuum robots," *Int. Jour. Robots. Res.*, vol. 29, no. 13, pp. 1661–1683, Jul. 2010.

[3] D. Trivedi, C. Rahn, W. Kier, and I. Walker, "Soft robotics: Biological inspiration, state of the art, and future research," *Applied Bionics and Biomechanics*, vol. 5, no. 2, pp. 99–117, Jun. 2008.

[4] I. Walker, "Continuous backbone "continuum" robot manipulators: A review," *ISRN Robotics*, vol. 2013, no. 1, pp. 1–19, Jul. 2013.

[5] E. Butler, R. Hammond-Oakley, S. Chawarski, A. Gosline, P. Codd, T. Anor, J. Madsen, P. Dupont, and J. Lock, "Robotic neuro-endoscope with concentric tube augmentation," in *Proc. IEEE/RSJ Int. Conf. Intel. Robot. Syst.*, Vilamoura, Portugal, 2012, pp. 2941–2946.

[6] Y. Chen, J. Liang, and I. Hunter, "Modular continuum robotic endoscope design and path planning," in *Proc. IEEE Int. Conf. Robot. Autom.*, Hong Kong, China, 2014, pp. 5393–5398.

[7] R. Buckingham, "Snake arm robots," *Ind. Robot: An Int. Jour.*, vol. 29, no. 3, pp. 242–245, Mar. 2002.

[8] M. Monapi, I. S. Godage, A. M. Vijaykumar, and I. Walker, "A novel continuum robotic cable aimed at applications in space," *Advanced Robotics*, vol. 29, no. 13, pp. 861–875, Jul. 2015.

[9] C. Laschi, B. Mazzolai, V. Mattoli, M. Cianchetti, and P. Dario, "Design of a biomimetic robotic octopus arm," *Bioinsp. and Biomim.*, vol. 4, no. 1, pp. 1–8, Jan. 2009.

[10] T. Mahl, A. Hildebrandt, and O. Sawodny, "A variable curvature continuum kinematics for kinematic control of the bionic handling assistant," *IEEE Transactions on Robotics*, vol. 30, no. 4, pp. 935–949, 2014.

[11] B. Jones and I. Walker, "Kinematics of multisection continuum robots," *IEEE Trans. Robot.*, vol. 22, no. 1, pp. 43–57, Feb. 2006.

[12] H. Mochiyama and H. Kobayashi, "The shape jacobian of a manipulator with hyper degrees of freedom," in *Proc. IEEE Int. Conf. Robot. Autom.*, Detroit, MI, 1999, pp. 2837–2842.

[13] I. Gravagne and I. D. Walker, "Manipulability, force, and compliance analysis for planar continuum manipulators," *IEEE Trans. Robots. Autom.*, vol. 18, no. 3, pp. 263–273, Jun. 2002.

[14] B. Jones and I. Walker, "A new approach to jacobian formulation for a class of multi-section continuum robots," in *Proc. IEEE Int. Conf. Robot. Autom.*, Barcelona, Spain, 2004, pp. 3279–3284.

[15] B. A. Jones, W. McMahan, and I. D. Walker, "Design and analysis of a novel pneumatic manipulator," in *Proc. IFAC Symposium on Mechatronic Systems*, Sydney, Australia, 2004, pp. 745–750.

[16] S. H. Sadati, S. E. Naghibi, I. D. Walker, K. Althoefer, and T. Nanayakkara, "Control space reduction and real-time accurate modeling of continuum manipulators using ritz and ritz–galerkin methods," *IEEE Robotics and Automation Letters*, vol. 3, no. 1, pp. 328–335, 2018.

[17] G. Gallot, O. Ibrahimand, and W. Khalil, "Dynamic modeling and simulation of a 3-d eel-like robot," in *Proc. IEEE Int. Conf. Robot. Autom.*, Rome, Italy, 2007, pp. 1486–1491.

[18] R. Kang, A. Kazakidi, E. Guglielmino, D. Branson, D. Tsakiris, J. Ekaterinaris, and D. Caldwell, "Dynamic modeling of a hyper-redundant octopus-like manipulator for underwater applications," in *Proc. IEEE/RSJ Int. Conf. Intel. Robot. Syst.*, San Francisco, CA, 2011, pp. 4054–4059.

[19] A. Marchese, R. Tedrake, and D. Rus, "Dynamics and trajectory optimization for a soft spatial fluidic elastomer manipulator," in *Proc. IEEE Int. Conf. Robot. Autom.*, Seattle, WA, 2015, pp. 2528–2535.

[20] E. Tatlicioglu, I. Walker, and D. Dawson, "Dynamic modeling for planar extensible continuum robot manipulators," *Int. Jour. Robot. Autom.*, vol. 24, no. 4, pp. 1087–1099, Apr. 2009.

[21] B. Conrad and M. Zinn, "Closed loop task space control of an interleaved continuum rigid manipulator," in *Proc. IEEE Int. Conf. Robot. Autom.*, Seattle, WA, 2015, pp. 1743–1750.

[22] R. Goldman, A. Bajo, and N. Simaan, "Compliant motion control for multisegment continuum robots with actuation force sensing," *IEEE Trans. Rob.*, vol. 30, no. 4, pp. 890–902, Apr. 2014.

[23] A. Kapadia, K. Fry, and I. Walker, "Empirical investigation of closed-loop control of extensible continuum manipulators," in *Proc. IEEE Int. Conf. Intell. Robot. Sys.*, Chicago, IL, 2014, pp. 329–335.

[24] S. Sadati, Y. Noh, S. Naghibi, and A. Althoefer, "Stiffness control of soft robotic manipulators for minimally invasive surgery (mis) using scale jamming," in *Int. Conf. Rob. and Autom.*, Amsterdam, The Netherlands, 2015, pp. 141–151.

[25] M. Yip and D. Camarillo, "Model-less feedback control of continuum manipulators in constrained environments," *IEEE Trans. Rob.*, vol. 30, no. 4, pp. 880–888, Apr. 2014.

[26] M. Csencsits, B. Jones, and W. McMahan, "User interfaces for continuum robot arms," in *Proc. IEEE Int. Conf. Intell. Robot. Sys*, Edmonton, Canada, 2005, pp. 3011–3018.

[27] A. Kapadia, I. Walker, and E. Tatlicioglu, "Teleoperation control of a redundant continuum manipulator using a non-redundant rigid-link master," in *Proc. IEEE Int. Conf. Intell. Robot. Sys.*, Algarve, Portugal, 2012, pp. 3105–3110.

[28] C. Frazelle, A. Kapadia, K. Fry, and I. Walker, "Teleoperation mappings from rigid link robots to their extensible continuum counterparts," in *Proc. IEEE Int. Conf. Robot. Autom.*, Stockholm, Sweden, 2016.

[29] C. Frazelle, A. Kapadia, and I. Walker, "Developing a kinematically similar master device for extensible continuum robot manipulators," *J. Mech. and Robot.*, vol. 10, no. 2, pp. 025 005–025 005–8, Apr. 2018.

[30] H.-S. Yoon and B.-J. Yi, "Design of a master device for controlling multi-moduled continuum robots," *Proceedings of the Institution of Mechanical Engineers, Part C: Journal of Mechanical Engineering Science*, vol. 231, no. 10, pp. 1921–1931, 2017.

[31] H. El-Hussieny, U. Mehmood, Z. Mehdi, S.-G. Jeong, M. Usman, E. W. Hawkes, A. M. Okamura, and J.-H. Ryu, "Development and evaluation of an intuitive flexible interface for teleoperating soft growing robots," in *2018 IEEE/RSJ International Conference on Intelligent Robots and Systems (IROS)*. IEEE, 2018, pp. 4995–5002.

[32] M. Mihelj and J. Podobnik, *Haptics for Virtual Reality and Teleoperation*. Dordrecht, Netherlands: Springer Science+Business Media, 2012.

[33] A. Okamura, "Haptic feedback in robot-assisted minimally invasive surgery," *Current Opinion in Urology*, vol. 19, no. 1, pp. 102–107, 2009.

[34] A. Talasaz, R. V. Patel, and M. D. Naish, "Haptics-enabled teleoperation for robot-assisted tumor localization," in *2010 IEEE International Conference on Robotics and Automation*, 2010, pp. 5340–5345.

[35] S. Hirche and M. Buss, "Human-oriented control for haptic teleoperation," *Proceedings of the IEEE*, vol. 100, no. 3, pp. 623–647, 2012.

[36] D. Escobar-Castillejos, J. Noguez, L. Neri, A. Magana, and B. Benes, "A review of simulators with haptic devices for medical training," *Journal of medical systems*, vol. 40, no. 4, p. 104, 2016.

[37] J. Winches. (2017, August) Slack rope detectors. [Online]. Available: http://www.jeamar.com/blocks/slack-rope-detectors/

[38] R. Coulson, M. Robinson, M. Kirkpatrick, and D. R. Berg, "Design and preliminary testing of a continuum assistive robotic manipulator," *Robotics*, vol. 8, no. 4, p. 84, 2019.

[39] H. In, H. Lee, U. Jeong, B. B. Kang, and K.-J. Cho, "Feasibility study of a slack enabling actuator for actuating tendon-driven soft wearable robot without pretension," in *2015 IEEE International Conference on Robotics and Automation (ICRA)*. IEEE, 2015, pp. 1229–1234.

[40] A. Yeshmukhametov, K. Koganezawa, and Y. Yamamoto, "A novel discrete wire-driven continuum robot arm with passive sliding disc: Design, kinematics and passive tension control," *Robotics*, vol. 8, no. 3, p. 51, 2019.

[41] A. Chawla, C. Frazelle, and I. Walker, "A comparison of constant curvature forward kinematics for multisection continuum manipulators," in *2018 Second IEEE International Conference on Robotic Computing (IRC)*. IEEE, 2018, pp. 217–223.

[42] Arduino. (2016, May) Arduino due. [Online]. Available: https://store.arduino.cc/usa/due

[43] B. A. Jones and I. D. Walker, "Limiting-case analysis of continuum trunk kinematics," in *Proc. IEEE Int. Conf. Robot. Auto.*, Rome, Italy, 2007, pp. 1363–1368.

[44] W. Felt, M. T. andT. Allen, G. Hein, J. Pompa, K. Albert, and D. Remy, "An inductance-based sensing system for bellows-driven continuum joints in soft robots," in *Robotics: Science and Systems*, The Hague, Netherlands, 07 2017.

[45] W. McMahan, M.Pritts, V. Chitrakaran, D. Dienno, M. Grissom, B. Jones, M. Csencsits, C. Rahn, D. Dawson, and I. Walker, "Fields trials and testing of octarm continuum robots," in *Proc. IEEE Int. Conf. Robot. Autom.*, Orlando, FL, 2006, pp. 2336–2341.